Novel highly conductive and transparent graphene based conductors

Ivan Khrapach, Freddie Withers, Thomas H. Bointon, Dmitry K. Polyushkin, William L. Barnes, Saverio Russo, and Monica F. Craciun*

Centre for Graphene Science, College of Engineering, Mathematics and Physical Sciences, University of Exeter, Exeter, EX4 4QL, UK

E-mail: m.f.craciun@exeter.ac.uk

Future wearable electronics, displays and photovoltaic devices require materials which are mechanically flexible, lightweight and low-cost, in addition to being electrically conductive and optically transparent [1–3]. Nowadays indium tin oxide (ITO) is the most wide spread transparent conductor in optoelectronic applications, however the mechanical rigidity of this material limits its use for future flexible devices. In the race to find novel transparent conductors, graphene monolayers and multilayers are the leading candidates as they have the potential to satisfy all future requirements. Graphene, one-atom-thick layer of carbon atoms, is transparent[4], conducting [5, 6], bendable [7] and yet one of the strongest known materials [8]. However, the use of graphene as a truly transparent conductor remains a great challenge because the lowest values of its sheet resistance (R_s) demonstrated so far are above the values of commercially available ITO (i.e. 10 $\Omega/\square$ at an optical transmittance Tr=85% [9]). Currently many efforts are concentrated on decreasing the R_s of graphene-based materials while maintaining a high Tr, which will allow their potential to be harnessed in optoelectronic applications. To date, the best values of sheet resistance and transmittance found in graphene-based materials are still far from the performances of ITO, with typical values of R_s=30 $\Omega/\square$ at Tr=90% for graphene multilayers [7, 12] and R_s=125 $\Omega/\square$ at Tr=97.7% for chemically doped graphene [7, 10, 11].

Here we report novel graphene-based transparent conductors with a sheet resistance of 8.8 $\Omega/\square$ at Tr=84%, a carrier density as high as $8.9\times10^{14}cm^{-2}$ and a room temperature carrier mean free path as large as $\sim 0.6\mu m$. These materials are obtained by intercalating few-layer graphene (FLG) with ferric chloride ($FeCl_3$) [13, 14]. Through a combined study of electrical transport and optical transmission measurements we demonstrate that $FeCl_3$ enhances the electrical conductivity of FLG while leaving these graphene-based materials highly transparent. We also show that $FeCl_3$-FLG are stable in air up to one year, which

1

demonstrates the potential of these materials for industrial production of transparent conductors. The unique combination of record low sheet resistance, high optical transparency and macroscopic room temperature mean free path has not been demonstrated so far in any other doped graphene system, and opens new avenues for graphene-based optoelectronics.

Pristine FLG ranging from two- to five-layers (2L to 5L) were obtained by micromechanical cleavage of natural graphite [5] on glass or SiO_2/Si. The number of layers composing each FLG was determined by optical contrast and Raman spectroscopy (see Supporting Information). The intercalation process with $FeCl_3$ was performed in vacuum with the two-zone vapor transport method [15]. $FeCl_3$ is sublimated in the lowest temperature zone and it diffuses to the higher temperature zone where the intercalation of FLG takes place (see Experimental section). The structural, electrical and optical characterization is carried out by means of three complementary experimental techniques: low-temperature charge transport, optical transmission and Raman spectroscopy.

Figure 1a shows the Raman spectra of pristine FLG on SiO_2/Si, with the G-band at 1580 cm^{-1} and the 2D-band at 2700 cm^{-1} [16, 17]. As expected for pristine FLGs, increasing the number of layers results in an increase of the G-band intensity [18], whereas the 2D-band acquires a multi-peak structure [16, 17]. The charge transfer from $FeCl_3$ to graphene modifies the Raman spectra of FLGs in two distinctive ways [13, 14, 19]: an upshift of the G-band and a change of the 2D-band from multi- to single-peak structure, respectively (see Figure 1a). The shift of the G-band to G_1=1612 cm^{-1} is a signature of a graphene sheet with only one adjacent $FeCl_3$ layer, whereas the shift to G_2=1625 cm^{-1} characterizes a graphene sheet sandwiched between two $FeCl_3$ layers [13–15] (see Figure 1a). The frequencies, linewidths and lineshapes of the G_1 and G_2 peaks do not depend on the number of graphene layers which indicates the decoupling of the FLGs into separate monolayers due to the intercalation of $FeCl_3$ between the graphene sheets. This is consistent with the changes in the 2D-band shape and with the Raman studies of other intercalants such as Potassium [20, 21] and Rubidium [21]. These observations allow us to identify the structure of intercalated 2L samples as one $FeCl_3$ layer sandwiched between the two graphene sheets. However, the structural determination of thicker $FeCl_3$-FLG cannot rely uniquely on the Raman spectra, it requires complementary knowledge from electrical transport experiments. Direct structural determination for example by X-ray diffraction would be valuable to confirm the findings of Raman and electrical transport measurements, however the small thickness of $FeCl_3$-FLG

2

and the substrate effects make it difficult to apply such technique to these systems.

To characterize the structure of thicker $FeCl_3$-FLG, we study the oscillatory behaviour of the longitudinal magneto-conductance (G_{xx}) in a perpendicular magnetic field (i.e. Shubnikov-de Haas oscillations, SdHO) in combination with the Hall resistance (R_{xy}). Here we discuss the representative data for an intercalated 5L sample patterned into a Hall bar geometry (see Figure 1c and Experimental section). Figure 1b shows SdHO of G_{xx} as a function of perpendicular magnetic field (B) for different temperatures. It is apparent that for T<10K G_{xx} oscillates with two distinct frequencies. For T>10K only the lower frequency oscillations are visible. These observations indicate that electrical conduction takes place through parallel gases of charge carriers with distinct densities. Indeed, the Fourier transform of $G_{xx}(1/B)$ yields peaks at frequencies $f_{SdHO_1} = 1100T$ and $f_{SdHO_2} = 55T$ (see Figure 1d), corresponding to charge carrier densities $n_1 = (1.07 \times 10^{14} \pm 5 \times 10^{11})cm^{-2}$ and $n_2 = (5.3 \times 10^{12} \pm 4 \times 10^{11})cm^{-2}$ (with $n_i = 4ef_{SdHO_i}/h$ [6, 22]).

The temperature dependence of the magneto-conductivity oscillations allows us to determine the cyclotron mass of the charge carriers in these parallel gases. Figures 1e and f show the low- and high-frequency magneto-conductivity oscillations for different temperatures (see Experimental section). In all cases, the temperature decay of the amplitude is well described by $A(T) \propto T/sinh(2\pi^2 k_B T m_c/\hbar e B)$ (see Figure 1g), with cyclotron masses $m_{c_1} = (0.25 \pm 0.05)m_e$ and $m_{c_2} = (0.08 \pm 0.001)m_e$ for the high- and low-frequency oscillations, respectively. These values correspond to the expected values of cyclotron mass for massless Dirac fermions $m_c = \sqrt{h^2 n/4\pi v_F^2} = 0.21m_e$ at n_1 and for chiral massive charge carriers of bilayer graphene $m_c = \sqrt{\hbar^2 v_F^2 \pi n + (\gamma/2)^2}/v_F^2 = 0.084m_e$ at n_2 (with $v_F = 10^6$m/s the Fermi velocity [6] and γ the interlayer hopping energy [15]), see Supporting Information. Therefore, intercalation of $FeCl_3$ decouples the stacked 5L graphene into parallel gases of massless (1L) and massive (2L) charge carriers.

The charge carrier type (electrons or holes) and the number of parallel gases present in $FeCl_3$-FLG is readily identified by correlating SdHO to the Hall resistance measurements. The linear dependence of $R_{xy}(B)$ with positive slope identifies charge carriers as holes, with a Hall carrier density $n_H = B/(eR_{xy}) = 3 \times 10^{14}cm^{-2}$ (see Figure 1c). Since the total carrier density $n_{tot} = \sum_i n_i$ should be higher than $n_H = (\sum_i n_i \mu_i)^2/\sum_i n_i \mu_i^2$ (with n_i and μ_i the carrier density and mobility of each hole gas) [23], only a minimum of three parallel hole gases with $n_1 = 1.07 \times 10^{14}cm^{-2}$ can explain the estimated value of n_H, i.e. $3 \times n_1 + n_2 \geq n_H$ (see
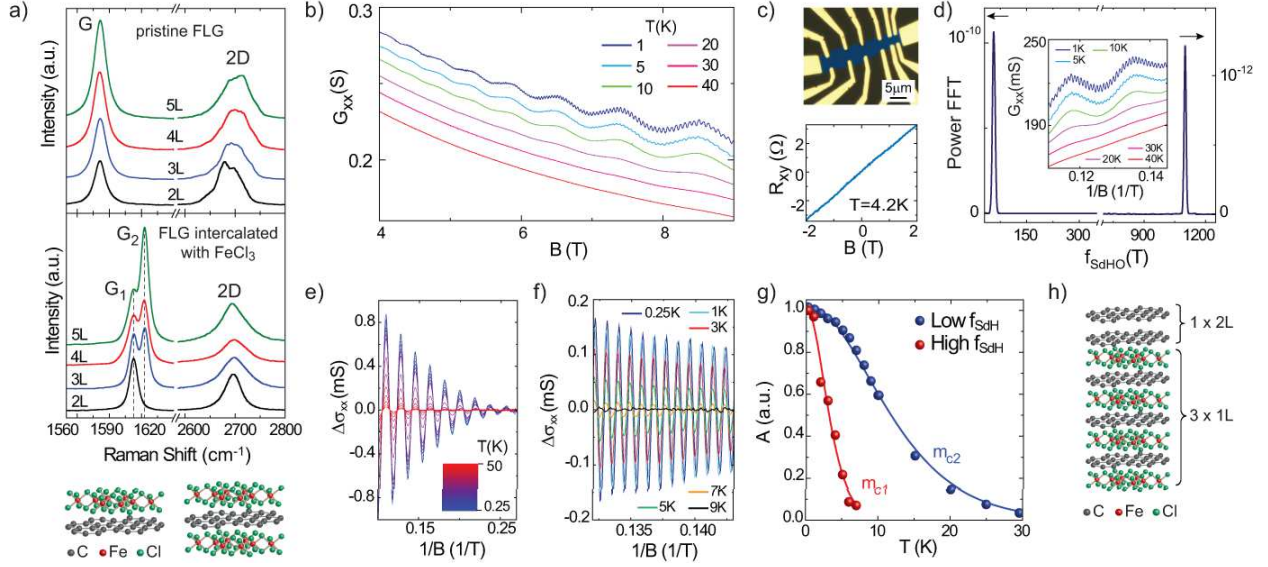
FIG. 1: a) The G and 2D Raman bands of pristine FLG (top) and of $FeCl_3$-FLG (bottom) with different thicknesses ranging from 2L to 5L. The Raman shift of G to G_1 and G_2 stem for a graphene sheet with one or two adjacent $FeCl_3$ layers as shown by the schematic crystal structure. b) Longitudinal conductance (G_{xx}) as a function of magnetic field at different temperatures (curves shifted for clarity). c) Top panel: optical microscope image of a Hall bar device. Bottom panel: Hall resistance (R_{xy}) as function of magnetic field. d) Fourier transform of $G_{xx}(1/B)$ with peaks at frequencies $f_{SdH}^{(1)} = 1100T$ and $f_{SdH}^{(2)} = 55T$. The inset shows G_{xx} as a function of inverse magnetic field at different temperatures (curves shifted for clarity). Panels e) and f), respectively, show the low- and high- frequency magneto-conductivity oscillations vs 1/B extracted from the measurements in b) (see Experimental section). g) Temperature decay of the amplitude (A) of $\Delta\sigma_{xx}$ oscillations at B=6.2T. The amplitudes are normalized to their values at T=0.25K. The continuous lines are fits to $A(T)/A(0.25)$ with the cyclotron mass m_c as the only fitting parameter. h) Schematic crystal structure of a 5L $FeCl_3$-FLG in which electrical transport takes place through four parallel conductive planes, one with bilayer character and three with monolayer character.

Supporting Information). Therefore, the electrical transport characterization demonstrates the presence of four parallel hole gases, of which one with bilayer character (and density n_2) and three with monolayer character (each with density n_1). These findings are confirmed by the Raman spectra taken after the device fabrication showing the presence of pristine G, G_1 and G_2 peaks (see Supporting Information). A schematic of this crystal structure

4

is illustrated in Figure 1h. The bilayer gas is likely to be caused by the first two layers of the stacking which have been de-intercalated due to rinsing in acetone during lift-off [19]. The bottom part of the stacking has a per-layer doping of $n_1 = 1.07 \times 10^{14} cm^{-2}$ and the stoichiometry of stage-1 $FeCl_3$ graphite intercalation compounds (i.e. where each graphene layer is sandwiched by two $FeCl_3$ layers) [15]. In total we have investigated electrical transport and Raman spectroscopy in more than 10 intercalated 5L samples and in all cases we confirmed the structure reported in Figure 1h.

A remarkable property of $FeCl_3$-FLGs shown by the electrical transport characterization is that intercalated materials thicker than 3L invariably exhibit a very low-sheet resistance, which is essential for their use as electrical conductors. We find a room temperature value of $R_s = 8.8\Omega/\square$ in 5L intercalated FLGs. The 4L intercalated FLGs typically exhibit higher sheet resistance values than the 5L intercalated samples with a similar crystal structure (see Supporting Information for a comparison between the electrical properties and Raman spectra of several 4L and 5L intercalated FLGs). Furthermore, the sheet resistance of $FeCl_3$-FLGs thicker than 2L decreases when lowering the temperature as expected for metallic conduction (see Figure 2a). Contrary to intercalated samples, pristine FLGs always have a higher R_s ($>120~\Omega/\square$) and they exhibit non-metallic behaviour as a function of temperature [5, 24, 25] (see Figure 2b). This suggests that the origin of the low values of R_s and the metallic nature of the conduction are consequences of intercalation with $FeCl_3$. $FeCl_3$-FLGs thinner than 3L suffer of partial de-intercalation during the device fabrication, which results in a non-metallic behaviour similar to pristine FLGs and in higher R_s values (see Figure 2a).

The low values of R_s characterizing thick $FeCl_3$-FLG are accompanied by an extremely high charge density. Indeed, the Hall coefficient measurements reveal that n_H ranges from $3 \times 10^{14} cm^{-2}$ to $8.9 \times 10^{14} cm^{-2}$, depending on the number of layers (see Figures 2c and d). These charge densities exceeds even the highest values demonstrated so far by liquid electrolyte [26] or ionic [27] gating. The corresponding charge carrier mobility for the 4L and 5L samples typically ranges from $\mu_H = 1540 cm^2/Vs$ to $\mu_H = 3650 cm^2/Vs$ ($\mu_H = 1/(n_H e\rho_{xx})$ with ρ_{xx} the longitudinal resistivity and e the electron charge). Consequently, the charge carriers in thick $FeCl_3$-FLG have a macroscopic mean free path as high as 0.6 μm in 5L at room temperature. The outstanding electrical properties, e.g. lower R_s than ITO and macroscopic mean free path, found in $FeCl_3$-FLGs thicker than 3L are of fundamental interest for the development of novel electronic applications based on highly conductive materials.
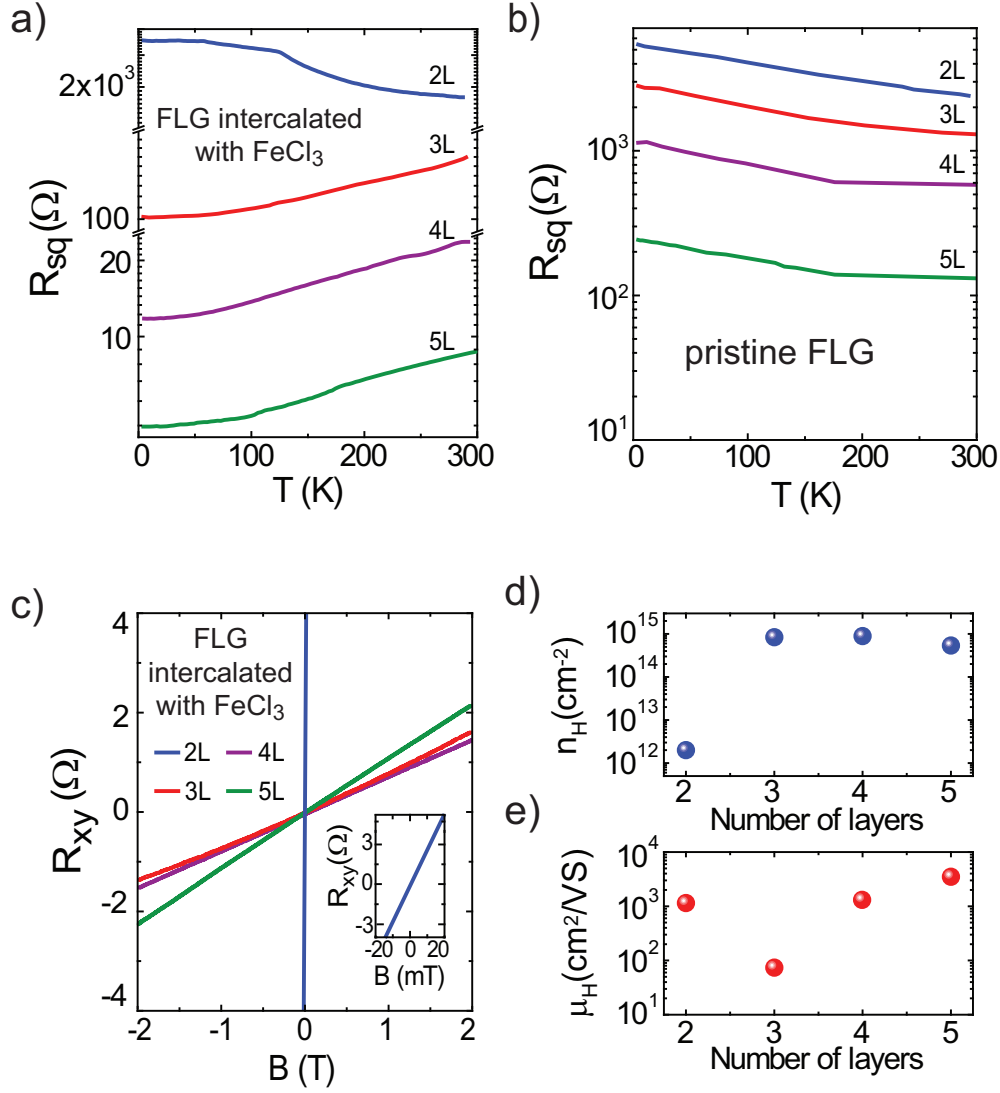
FIG. 2: a) Temperature dependence of the square resistance for $FeCl_3$-FLG of different thicknesses. b) Square resistance for pristine FLG of different thicknesses as function of temperature. These devices are fabricated on SiO_2/Si substrates and the highly-doped Si substrate is used as a gate to adjust the Fermi level to the charge neutrality of the system. c) Hall resistance of $FeCl_3$-FLG as a function of magnetic field. The inset shows the data for the bilayer sample on a smaller B scale. Panels d) and e) show the carrier density and mobility for $FeCl_3$-FLG as a function of the number of graphene layers.

Whether $FeCl_3$-FLGs can replace ITO in optoelectronic applications strongly depends on their optical properties. Surprisingly, our detailed study of the optical transmission in the visible wavelength range shows that while $FeCl_3$ intercalation improves significantly the

electrical properties of graphene, it leaves the optical transparency nearly unchanged. Figures 3a and b show a comparison between the transmittance spectra of pristine FLG and $FeCl_3$-FLG. The transmittance values of pristine FLG at the wavelength of 550nm are in agreement with the expected values [4], highlighted in Figure 3a, and with the results reported by other groups [4, 7]. Upon intercalation, the transmittance slightly decreases at low wavelengths, but it is still above 80 %. In order to measure an accurate value of transmittance we fit it with a linear dependence on the number of layers for a statistical ensemble of flakes (Figure 3d). This results in similar extinction coefficients per layer for pristine FLG ($\approx 2.4\pm0.1\%$) and for $FeCl_3$-FLG ($\approx 2.6\pm0.1\%$), see Figure 3d. For wavelengths longer than 550nm we observe an increase in the optical transparency of $FeCl_3$-FLG. This is a significant advantage of our material compared to ITO whose transparency decreases for wavelengths longer than 600nm [2]. This property will provide useful applications that require conductive electrodes which are transparent both in visible and near infrared range. For instance, $FeCl_3$-FLG transparent electrodes could be used for solar cells to harvest energy over an extended wavelength range as compared to ITO-based devices, or for electromagnetic shielding in infrared.

The high transparency observed in $FeCl_3$-FLG complemented by their remarkable electrical properties make these materials valuable candidates for transparent conductors. However, to replace ITO in optoelectronic applications, it is generally agreed that materials must (at least) have the properties of commercially available ITO (R_s=10 $\Omega/\square$ and Tr=85% [9]). Figure 3e compares R_s *vs.* Tr of $FeCl_3$-FLG materials with ITO [28], and other promising carbon-based candidates to replace ITO such as carbon-nanotube films [29] and doped graphene materials [7]. It is apparent that R_s and Tr of $FeCl_3$-FLGs outperform the current limits of ITO and of the best values reported so far for doped graphene [7]. Therefore, the outstandingly high electrical conductivity and optical transparency make $FeCl_3$-FLG materials the best transparent conductors for optoelectronic devices.

Finally, an important characteristic required by a transparent conductor is its stability upon exposure to air. In principle FLGs could be intercalated with a large variety of molecules, similar to the graphite intercalation compounds (GIC) [15]. However, most of the GIC are unstable in air, with donor compounds being easily oxidized and acceptors being easily desorbed. Therefore we studied the stability in air of $FeCl_3$-FLG by performing Raman measurements as a function of time. We found that the Raman spectra of $FeCl_3$-FLG
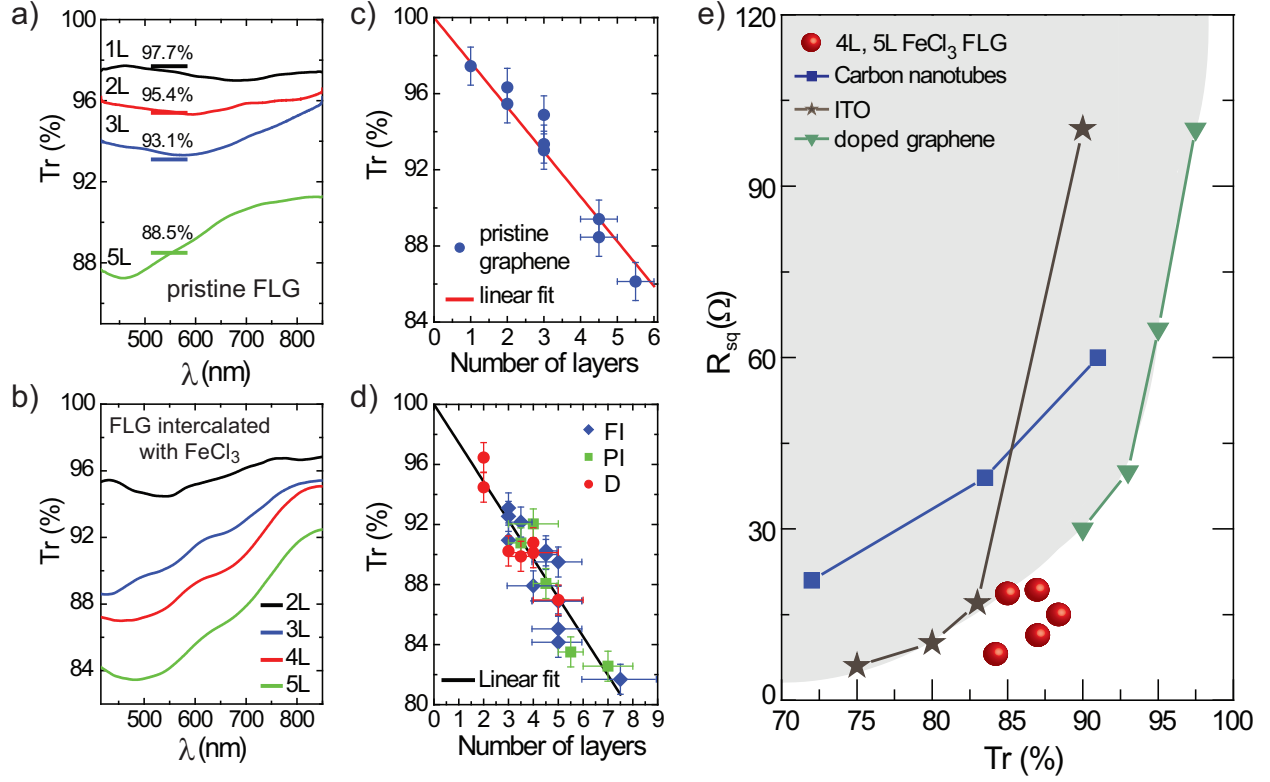
FIG. 3: Panels a) and b) show the transmittance spectra of pristine FLG and FeCl$_3$-FLG, respectively. The horizontal lines in b) are the corresponding transmittances at the wavelength of $550nm$ reported in the literature [4, 7]. c) Transmittance at $550nm$ for pristine FLG as a function of the number of layers. The red line is a linear fit, which gives the extinction coefficient of $2.35\pm0.1\%$ per layer. d) Transmittance at $550nm$ for fully intercalated FeCl$_3$-FLG (FI), partially intercalated FeCl$_3$-FLG (PI) and doped FeCl$_3$-FLG (D) as a function of the number of layers. The black line is a linear fit with the extinction coefficient of $(2.6\pm0.1)\%$ per layer. e) Square resistance *versus* transmittance at $550nm$ for 4L and 5L FeCl$_3$-FLG (from these experiments), ITO (from [28]), carbon-nanotube films (from ref [29]) and doped graphene materials (from ref [7]). FeCl$_3$-FLG outperform the current limit of transparent conductors, which is indicated by the grey area.

samples show no appreciable changes on a time scale of up to one year (see Supporting Information). This property has important implications for the utilization of these materials as transparent conductors in practical applications such as displays and photovoltaic devices.

In conclusion, we demonstrate novel transparent conductors based on few layer graphene intercalated with ferric chloride with an outstandingly high electrical conductivity and

optical transparency. We show that upon intercalation a record low sheet resistance of 8.8 $\Omega/\square$ is attained together with an optical transmittance higher than 84% in the visible range. These parameters outperform the best values of ITO and of other carbon-based materials. The $FeCl_3$-FLGs materials are relatively inexpensive to make and they are easily scalable to industrial production of large area electrodes. Contrary to the numerous chemical species that can be intercalated into graphite (more than hundred [15]), many of which are unstable in air, we found that $FeCl_3$-FLGs are air stable on a timescale of at least one year. Other air stable graphite intercalated compounds can only by synthesized in the presence of Chlorine gas [15], which is highly toxic. On the contrary, here we demonstrate that the intercalation of FLG with $FeCl_3$ is easily achieved without the need of using Chlorine gas, which ensures an environmental friendly industrial processing. Furthermore, the low intercalation temperature (360℃) required in the processing allows the use of a wide range of transparent flexible substrates which are compatible with existing transparent electronic technologies. These technological advantages combined with the unique electro-optical properties found in $FeCl_3$-FLG make these materials a valuable alternative to ITO in optoelectronics.

Experimental section

Sample fabrication. The intercalation process with $FeCl_3$ is performed in vacuum. Both anhydrous $FeCl_3$ powder and the substrate with exfoliated FLG are positioned in different zones inside a glass tube. The tube is pumped down to $2 \times 10^{-4} mbar$ at room temperature for 1 hour to reduce the contamination by water molecules. Subsequently, the FLG and the powder are heated for 7.5 hours at 360℃ and 310℃, respectively. A heating rate of 10℃/min is used during the warming and cooling of the two zones. Ohmic contacts are fabricated on $FeCl_3$-FLG by means of electron-beam lithography and lift-off of thermally evaporated chrome/gold bilayer (5/50 nm). We have fabricated $FeCl_3$-FLG on both SiO_2/Si and glass substrates and we found no significant differences in their transport properties.

Raman measurements. Raman spectra are collected in ambient air and at room temperature with a Renishaw spectrometer. An excitation laser with a wavelength of 532 nm, focused to a spot size of 1.5 μm diameter and a ×100 objective lens are used. To avoid sample damage or laser induced heating, the incident power is kept at 5 mW.

Electrical measurements. The longitudinal and the Hall resistances are studied in a

4-probe configuration by applying an a.c. current bias and measuring the resulting longitudinal and transversal voltages with a lock-in amplifier. The excitation current is varied to ensure that the energy range where electrical transport takes place is smaller than the energy range associated to the temperature of the electrons. This prevents heating of the electrons and the occurrence of nonequilibrium effects. Since conductances are additive, the analysis of Shubnikov-de Haas oscillations is performed on the longitudinal conductivity $\sigma_{xx} = \rho_{xx}/[\rho_{xx}^2 + \rho_{xy}^2]$ (with ρ_{xx} and ρ_{xy} the longitudinal and transversal resistivity, respectively). The low frequency magneto-conductivity oscillations shown in Figure 2d are obtained by averaging out the high frequency oscillations, whereas to obtain the high frequency oscillations shown in Figure 2e we subtract the low frequency oscillations from the longitudinal conductivity.

Transmission measurements. The transmission of pristine FLG and FeCl$_3$-FLG is characterized by measuring the bright-field transmission spectra. A system based on an inverted optical microscope (Nikon Eclipse TE2000-U) combined with a spectrometer and CCD camera (Princeton Instruments, SpectraPro 2500i) is used to acquire data. White light from a tungsten filament lamp is used to illuminate the samples and, after passing through the sample, is collected by a dry Nikon lens (S Plan Fluor ELWD) ×40 of NA 0.60. A slit width of 50 μm is used for the spectrometer, yielding a spectral resolution < 1 nm for the measurements. In the spectrometer the dispersed light is projected onto the 1024 by 256 lines of the CCD camera. Data from the camera are extracted to give the transmission spectra of the flake, or part of it, the data being normalized to the signal obtained through a region of bare substrate. For the visually uniform parts of the flakes, spectra are averaged along several lines of the CCD camera to improve the signal-to-noise ratio.

Supporting information.

Supporting information is available from the Wiley Online Library (http://onlinelibrary.wiley.com/doi/10.1002/adma.201200489/suppinfo) or from the author

----

[1] A. Kumar, C. Zhou, *ACS Nano* **2010**, 4, 11.

[2] D. S. Hecht, L. Hu, G. Irvin, *Adv. Mater.* **2011**, 23, 1482.

[3] J. K. Wassei, R. B. Kaner, *Materials today* **2010**, 13, 52.

[4] R. R. Nair, P. Blake, A. N. Grigorenko, K. S. Novoselov, T. J. Booth, T. Stauber, N. M. R. Peres, A. K. Geim, *Science* **2008**, 320, 1308.

[5] K. S. Novoselov, A. K. Geim, S. V. Morozov, D. Jiang, Y. Zhang, S. V. Dubonos, I. V. Grigorieva and A. A. Firsov, *Science* **2004**, 306, 666.

[6] K. S. Novoselov, K. S. Novoselov, A. K. Geim, S. V. Morozov, D. Jiang, M. I. Katsnelson, I. V. Grigorieva, S. V. Dubonos, A. A. Firsov, *Nature* **2005**, 438, 197.

[7] S. Bae, H. Kim, Y. Lee, X. Xu, J.-S. Park, Y. Zheng, J. Balakrishnan, T. Lei, H. R. Kim, Y. I. Song, Y.-J. Kim, K. S. Kim, B. Ozyilmaz, J.-H. Ahn, B. H. Hong, S.Iijima, *Nature Nanotechnol.* **2010**, 5, 574.

[8] C. Lee, X. Wei, J.W. Kysar, J. Hone, *Science* **2008**, 321, 385.

[9] S. De, J. N. Coleman, *ACS Nano* **2010**, 4, 2713.

[10] K. K. Kim, A. Reina, Y. Shi, H. Park, L.-J. Li, Y. H. Lee, and J. Kong, *Nanotechnology* **2010**, 21, 285205.

[11] A. Kasry, M. A. Kuroda, G. J. Martyna, G. S. Tulevski, A. A. Bol, *ACS Nano.* **2010**, 4, 3839.

[12] Y. Wang, S. W. Tong, X. F. Xu, B. Ozyilmaz, K. P. Loh, *Adv. Mater.* **2011**, 1514.

[13] W. Zhao, P. H. Tan, J. Liu, A. C. Ferrari, *J. Am. Chem. Soc.* **2011**, 133, 5941.

[14] D. Zhan, L. Sun, Z. H. Ni, L. Liu, X. F. Fan, Y. Wang, T. Yu, Y. M. Lam, W. Huang, Z. X. Shen, *Adv. Func. Mat.* **2010**, 20, 3504.

[15] M. S. Dresselhaus, G. Dresselhaus, *Adv. Phys.* **2002**, 51, 1.

[16] A. C. Ferrari, J. C. Meyer, V. Scardaci, C. Casiraghi, M. Lazzeri, F. Mauri, S. Piscanec, D. Jiang, K. S. Novoselov, S. Roth, A. K. Geim, *Phys. Rev. Lett.* **2006**, 97, 187401.

[17] L.M. Malard, M.A. Pimenta, G. Dresselhaus, M.S. Dresselhaus, *Physics Reports* 2009, 473, 51.

[18] Y. K. Koh, M.-H. Bae, D. G. Cahill, E. Pop, *ACS Nano* **2011**, 5, 269.

[19] N. Kim, K. S. Kim, N. Jung, L. Brus, P. Kim, *Nano Lett.* **2011**, 11, 860.

[20] C. A. Howard, M. P. M. Dean, F. Withers, *Phys. Rev. B* **2011**, 84, 241404(R).

[21] N. Jung, B. Kim, A. C. Crowther, N. Kim, C. Nuckolls, L Brus, *ACS Nano* **2011**, 5, 5708.

[22] Y. Zhang, Y.-W. Tan, H. L. Stormer, P. Kim, *Nature* **2005**, 438, 201.

[23] J. H. Davies, *The physics of low-dimentional semiconductors* (Cambridge Univ. Press, Cambridge, 1998)

[24] M. F. Craciun, S. Russo, M. Yamamoto, J. B. Oostinga, A. F. Morpurgo, S. Tarucha, *Nature Nanotech.* **2009**, 4, 383.

[25] W. Zhu, V. Perebeinos, M. Freitag, P. Avouris, *Phys. Rev. B* **2009**, 80, 235402.

[26] D. K. Efetov, P. Kim. *Phys. Rev. Lett.* **2010**, 105, 256805.

[27] J. Ye, M. F. Craciun, M. Koshino, S. Russo, S. Inoue, H. Yuan, H. Shimotani, A.F. Morpurgo, Y. Iwasa, *PNAS* **2011**, 108, 13002.

[28] J.-Y. Lee, S. T. Connor, Y. Cui, P. Peumans, *Nano Lett.* **2008**, 8, 689.

[29] D. S. Hecht, A. M Heintz, R.Lee, L. Hu, B. Moore, C. Cucksey, S. Risser, *Nanotechnology* **2010**, 22, 075201.